AIAA 80-1254R

Shock-Capturing Model for One- and Two-Phase Supersonic Exhaust Flow

Sanford M. Dash*
Science Applications, Inc., Princeton, N.J.
and
Roger D. Thorpe†
Aeronautical Research Associates of Princeton, Inc., Princeton, N.J.

A shock-capturing model (SCIPPY) for analyzing steady supersonic flows in two spatial dimensions is discussed. SCIPPY serves as a component part of the new JANNAF standard low-altitude rocket plume model as well as the NASA Langley Research Center model for aircraft afterbody flow. Generalized one- or two-phase mixtures are considered with a nonequilibrium treatment of gas/particle interactions implemented. Unique capabilities include the automated analysis of embedded subsonic regions behind Mach disks and the use of multiple-mapped domains for obtaining high grid resolution in strong wave regions. Applications to exhaust plume flowfields are stressed herein.

Introduction

THE SCIPPY shock-capturing model which analyzes steady supersonic flows in two spatial dimensions is described. SCIPPY was formulated to serve as a component part of the JANNAF standard low-altitude ($h < 70$ km) rocket plume model[1-3] presently under development. Rocket plumes contain multiple discontinuities and require the consideration of complex chemical, turbulence, and two-phase flow processes as well as embedded subsonic zones. The JANNAF model implements a modular approach[4] in which the plume is subdivided into a number of regions and each region is analyzed by computational techniques best descriptive of the dominant gasdynamic processes and length scales characterizing that region. In the plume nearfield, viscous (turbulent mixing) processes are generally confined to thin shear layers, permitting the use of a weakly interactive overlaid approach[5] in which viscous and inviscid processes are uncoupled. Here, SCIPPY serves as the inviscid component of the JANNAF model and is used to predict the underexpanded jet shock structure. SCIPPY fills the same role in the NASA/LRC patched component model[6,7] for predicting aircraft afterbody/exhaust flows.

For the analysis of wave processes in thick mixing regions, a fully coupled viscous version of SCIPPY is under development. This version integrates the parabolized Navier-Stokes equations via an explicit spatial marching procedure. Preliminary single-phase calculations[8,9] have been performed for fundamental interactive processes (i.e., the interaction of shock waves and expansion fans with supersonic shear layers) as well as for nonreactive plumes.

While SCIPPY was formulated for plume-related problems, its structure permits its usage for generalized supersonic flow problems, e.g., versions of SCIPPY have been developed for nozzle and diffuser flows,[10] and in-house calculations have been performed for a variety of external flows. This article will be confined to describing the inviscid version of the SCIPPY code, stressing applications to exhaust flowfields. The inviscid version has been extensively tested for single-phase flows and is operational for two-phase flows. Its principal features are:

1) The equations are cast in conservation form and solved by the two-step MacCormack algorithm.[11] Via this approach, internal shock waves in the flow are numerically captured. The conservation approach facilitates the analysis of complex real gas flows with nonequilibrium (chemistry and/or gas/particle) effects. The extension of this conservative approach to viscous supersonic flows[8,9] is quite straightforward. A strong argument for adaption of this approach involves its applicability to complex three-dimensional flowfields. Shock-capturing procedures have been demonstrated to predict extremely complex three-dimensional nozzle/exhaust flowfields[12,13] which are not readily analyzed by present characteristic or nonconservative finite-difference procedures.

2) A mapped multiple-domain approach is employed. This approach permits dividing the flowfield into a number of contiguous domains (bounded by shock, slipstream, or characteristic surfaces) which are analyzed either sequentially or simultaneously. Appropriate mappings permit high grid resolution in strong gradient regions. The bounding discontinuity surfaces are fitted.

3) Characteristic procedures are implemented at all boundary points. Present finite-difference procedures cannot rival the accuracy of characteristic techniques for a boundary point calculation.[14] To account for the entropy rise associated with captured shock reflections at boundary points, a nonisentropic pressure-density relation[13] is implemented.

4) A fully automated procedure is implemented for analyzing Mach disks. The one-dimensional streamtube approach suggested by Abbett[15] and implemented in the earlier inviscid plume model of Salas[16] is used.

5) The fully coupled treatment of nonequilibrium gas/particle interactions is performed via a direct extension of the basic shock-capturing procedure. This approach[17] is considerably more straightforward than that required in characteristic codes having comparable particle capabilities. It also provides several significant computational advantages over characteristic procedures.

Governing Equations

Conservation Equations for Two-Phase Flow

The extension of the standard single-phase conservation equations to analyze two-phase (gas/particle) flow in the nonequilibrium limit involves: 1) the introduction of gas/particle interaction terms as forcing functions in the gas-phase equations, which account for the exchange of momentum and energy between the gas and particles, and 2)

Presented as Paper 80-1254 at the AIAA/SAE/ASME 16th Joint Propulsion Conference, Hartford, Conn., June 30-July 2, 1980; submitted July 28, 1980; revision received Feb. 17, 1981.

*Assistant Division Manager. Member AIAA.
†Consultant. Member AIAA.

the solution of a system of differential equations for the particles based on a "continuum particle cloud" assumption where the continuous distribution of particle sizes at each point in the flow is modeled by several groups of representative "constant size" particles.

The coupled system of gas-phase and particle-cloud conservation equations[10,18] in Cartesian and cylindrical coordinates is given as:

$$\frac{\partial E}{\partial x}+\frac{\partial F}{\partial y}+G=0 \tag{1}$$

where

$$E(k)=\begin{bmatrix} e_1 \\ e_2 \\ e_3 \\ e_4 \\ e_{5_i} \\ e_{6_j} \\ e_{7_j} \\ e_{8_j} \\ e_{9_j} \end{bmatrix} = \begin{bmatrix} \rho U \\ P+\rho U^2 \\ \rho UV \\ \rho UH \\ \rho U\alpha_i \\ \rho_{p_j}U_{p_j} \\ \rho_{p_j}U^2{}_{p_j} \\ \rho_{p_j}U_{p_j}V_{p_j} \\ \rho_{p_j}U_{p_j}h_{p_j} \end{bmatrix}; \quad F(k)=\begin{bmatrix} \rho V \\ \rho UV \\ P+\rho V^2 \\ \rho VH \\ \rho V\alpha_i \\ \rho_{p_j}V_{p_j} \\ \rho_{p_j}U_{p_j}V_{p_j} \\ \rho_{p_j}V^2{}_{p_j} \\ \rho_{p_j}V_{p_j}h_{p_j} \end{bmatrix}$$

and

$$G(k)=\begin{bmatrix} 0 \\ \Sigma\rho_{p_j}A_{p_j}(U-U_{p_j}) \\ \Sigma\rho_{p_j}A_{p_j}(V-V_{p_j})-JPy^{-1} \\ \Sigma\rho_{p_j}\{A_{p_j}[\bar{Q}\cdot(\bar{Q}-\bar{Q}_{p_j}) \\ -(\bar{Q}-\bar{Q}_{p_j})^2]+B_{p_j}(T-T_{p_j})\} \\ 0 \\ 0 \\ -\rho_{p_j}A_{p_j}(U-U_{p_j}) \\ -\rho_{p_j}A_{p_j}(V-V_{p_j}) \\ -\rho_{p_j}B_{p_j}(T-T_{p_j}) \end{bmatrix}+\frac{JF(k)}{y}$$

In these relations, the chemistry is assumed frozen and standard assumptions are used in describing the particles (namely, the particles are spherical, inert, occupy a negligible volume, and do not interact with one another). The subscript p designates particle variables, the subscript j distinguishes the particle size groups, and the subscript i distinguishes the chemical species whose mass fraction is α_i. U and V are the velocity components in the x (axial) and y (radial) directions, Q is the total velocity, ρ the density, H the total enthalpy, h the static enthalpy, and T the temperature. The parameter J is set equal to 0 for Cartesian coordinates and 1 for cylindrical coordinates.

Drag and Heat-Transfer Coefficients

The empirically determined drag and heat-transfer coefficients, C_{D_j} and Nu_j, are contained in the parameters A_{p_j} and B_{p_j} given by

$$A_{p_j}=\frac{3\mu}{16\rho_s}\left(\frac{C_D Re_p}{r_p}\right)_j \tag{2a}$$

and

$$B_{p_j}=\frac{3\mu C_p}{2\rho_s Pr}\left(\frac{Nu}{r_p}\right)_j \tag{2b}$$

Re_p is the lag Reynolds number given by

$$Re_{p_j}=\frac{2\rho}{\mu}r_{p_j}|\bar{Q}-\bar{Q}_{p_j}| \tag{3}$$

where μ, Pr, and C_p are the laminar viscosity, Prandtl number, and specific heat of the gas-phase mixture, respectively, ρ_s is the particle material density (a property of particle composition only, which should be distinguished from the particle-cloud density ρ_p, which is a measure of the local particle concentration), and r_{p_j} is the particle radius of the jth size group. The Nusselt number, Nu_j, is given by[19]

$$Nu_j=Nu_{0_j}(1+3.42M_{p_j}Nu_{0_j}/Re_{p_j}Pr)^{-1} \tag{4}$$

where

$$Nu_{0_j}=2+0.46Re_{p_j}{}^{0.55}Pr^{0.33}$$

and the lag Mach number, M_{p_j}, is given by

$$M_{p_j}=|\bar{Q}-\bar{Q}_{p_j}|(\gamma P/\rho)^{-1/2} \tag{5}$$

The drag coefficient is given by a functional relation of the form

$$C_{D_j}=C_{D_j}(Re_{p_j},M_{p_j},T_{p_j}/T,\gamma) \tag{6}$$

The recent study of Salita[20] has indicated that the drag relations of Hermsen[21] and Henderson[22] yield best overall agreement with experimental data for conditions encounterable in nozzle/exhaust flows. These relations have been incorporated in SCIPPY as detailed in Refs. 10 and 18.

Characteristic Equations for Two-Phase Flow

The conservation equations given above are supplemented by gas-phase characteristic relations which are used at boundary points. The characteristic directions for wave propagation are the (frozen) Mach lines, $\lambda^{\pm}$, given by

$$dy/dx=\lambda^{\pm}\equiv\tan(\theta\pm\mu) \tag{7}$$

where θ is the streamline direction ($\tan\theta=V/U$), and μ is the Mach angle ($\sin\mu=1/M$). The compatibility relations along $\lambda^{\pm}$ are given by

$$(\sin\mu\cos\mu/\gamma)\,d\ell nP\pm d\theta+F^{\pm}\,dx=0 \tag{8}$$

where the forcing function, $F^{\pm}$, contains the gas/particle interaction terms and is given by

$$F^{\pm}=\frac{J\sin\theta\sin\mu}{y\cos(\theta\pm\mu)}\pm\frac{\sin^2\mu}{\gamma p}$$
$$\times\sum_j\rho_{p_j}\left[A_{p_j}\left\{(V-V_{p_j})-(U-U_{p_j})\tan(\theta\pm\mu)+\frac{(\gamma-1)}{Q\sin\mu\cos\theta}\right.\right.$$
$$\left.\left.\times[(U-U_{p_j})^2+(V-V_{p_j})^2]\right\}+\frac{(\gamma-1)B_{p_j}}{Q\sin\mu\cos\theta}(T_{p_j}-T)\right] \tag{9}$$

The gas-phase streamlines are also characteristic directions

along which the following differential relations apply:

$$d\ell n\rho = d\ell nP^{1/\gamma} - \frac{(\gamma-1)}{\gamma PU}\sum_j \rho_{p_j}[A_{p_j}\{(U-U_{p_j})^2 + (V-V_{p_j})^2\} + B_{p_j}(T_{p_j}-T)]dx \quad (10)$$

$$dH = \Sigma\rho_{p_j}[A_{p_j}\{(U-U_{p_j})^2 + (V-V_{p_j})^2 - U(U-U_{p_j}) - V(V-V_{p_j})\} + B_{p_j}(T_{p_j}-T)]dx/\rho U \quad (11)$$

Equation (10) is the pressure-density relation along a streamline which would express the constancy of entropy for a single-phase flow. To account for entropy effects associated with captured shock-boundary interactions,[13] an additional term is added expressing the change in entropy (due to gas-phase processes only) at the adjacent grid point (determined via the shock-capturing solution of the conservation equations which yields the appropriate entropy change). Equation (11) yields the variation of total enthalpy along a streamline due to gas/particle interactions.

Thermodynamic Relations

The gas-phase static enthalpy, h, is given by the summation

$$h(\alpha_i, T) = \sum_i \alpha_i h_i(T) \quad (12)$$

where $h_i(T)$ is expressed by polynomial fits using the coefficients of Ref. 23, accessed from a thermochemical data bank.[24] For uniform composition flows, the species summation is performed a priori in a preprocessing routine. The specific heat capacity, C_p, is given by the temperature derivative of Eq. (12) and the specific heat ratio, γ, is given by

$$\gamma = \frac{C_p W/R_0}{C_p W/R_0 - 1} \quad (13)$$

where W is the gas-phase mixture molecular weight ($W=[\Sigma\alpha_i/m_i]^{-1}$) and R_0 is the universal gas constant. The equation of state

$$P = \rho(R_0/W)T \quad (14)$$

relates gas-phase properties only. The particle-cloud total enthalpy is given by

$$h_{p_j}(T_{p_j}) = \int C_s(T_{p_j})\,dT \quad (15)$$

It has been assumed that the particles are all of the same composition. This restriction is presently being removed to permit the analysis of several types of particles, each type being subdivided into representative size groups.

Computational Techniques

Multiple-Mapped Domains

SCIPPY is structured so that the overall flowfield is segmented into a number of contiguous domains bounded by principal discontinuity and/or solid surfaces. Each domain is solved in mapped coordinates (ξ,η) defined by the transformation

$$\xi = x \quad (16a)$$

$$\eta = (y-y_L(x))/(y_U(x)-y_L(x)) \quad (16b)$$

where y_U and y_L define the domain's upper and lower boundary geometry. The conservation equations in mapped coordinates are written

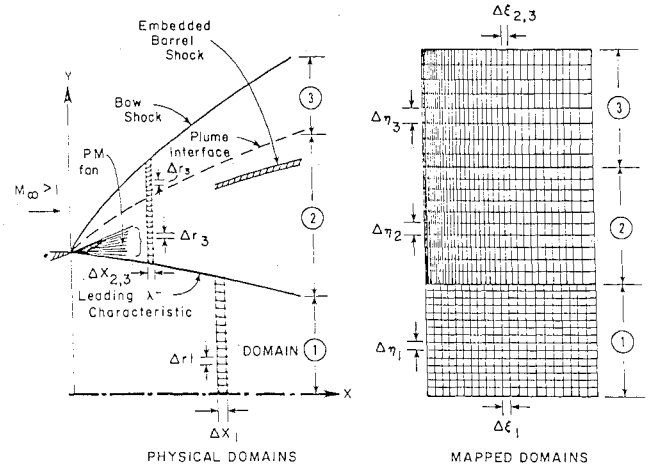

Fig. 1 Multiple-domain grid distribution in plume nearfield.

$$\frac{\partial E}{\partial\xi} + \frac{\partial\bar{F}}{\partial\eta} + \bar{G} = 0 \quad (17)$$

where

$$\bar{F} = bF - aE$$

$$\bar{G} = a_\eta E + G$$

$$a(\xi,\eta) = \frac{(1-\eta)y_L'(x) + \eta y_U'(x)}{y_U(x) - y_L(x)}$$

$$b(\xi) = (y_U(x) - y_L(x))^{-1}$$

The domains may be solved sequentially or simultaneously depending upon the specific segmenting employed, which is problem-dependent.

Consider, for example, the lip region of an underexpanded plume exhausting into a supersonic external stream (Fig. 1). The flowfield is typically segmented into three domains.‡ Domains 1 and 2 are separated by the leading downrunning characteristic, λ^-, emanating from the nozzle lip while domains 2 and 3 are separated by the inviscid plume interface. Domain 1 is calculated a priori with predicted properties along λ^- saved for use in calculating domain 2. Domains 1 and 2 are combined into a single domain a short distance (i.e., an exit radius) downstream of the nozzle exit plane. Domains 2 and 3 are calculated simultaneously employing the same integration step, ΔX. Both of these domains are triangular and the mapping provides high spatial resolution in the immediate lip region where gradients are quite severe. Shocks embedded within any of these domains are captured, including the barrel shock which can be a very strong discontinuity (i.e., pressure ratios can exceed 100:1 for highly underexpanded plumes). Boundary discontinuities such as the bow shock and plume interface are fitted.

Interior Point Integration

A fixed number of equally spaced grid intervals, $\Delta\eta$, spans each domain. The two-step MacCormack algorithm[11] applied to Eq. (17) for the integration step, $\Delta\xi$, yields

Predictor step:

$$\bar{E}_I = E_I^k - \frac{\Delta\xi}{\Delta\eta}[(1-\epsilon)F_I^{k+1} - (1-2\epsilon)F_I^k - \epsilon F_{I-1}^k] - G_I^k\Delta\xi \quad (18a)$$

‡The external flow is often represented by simple pressure-flow deflection rules (to be discussed) eliminating domain 3. If the degree of underexpansion is small and/or if exit conditions are near sonic, a single domain is employed to analyze the plume.

Corrector step:

$$E_I^{k+1} = \frac{1}{2}\left\{E_I^k + \tilde{E}_I - \frac{\Delta\xi}{\Delta\eta}\left[\epsilon\tilde{F}_{I+1} + (1-2\epsilon)\tilde{F}_I + (\epsilon-1)\tilde{F}_{I-1}\right] - \tilde{G}_I\Delta\xi\right\} \quad (18b)$$

Note that the bar over the F and G arrays of Eq. (17) has been dropped for clarity. In these difference equations, I is the radial grid point indicator, k designates properties at ξ and $k+1$ at $\xi+\Delta\xi$, $\sim$ designates provisional values (properties determined in the predictor step), and ϵ is varied between 0 and 1 at subsequent steps for a nonpreferential treatment of wave propagation.

The inclusion of particles does not alter the basic integration approach employed for single-phase flows. The step size, $\Delta\xi$, is based on gas-phase properties only and is determined via the use of formal characteristic intersections[10,18] rather than a linearized stability relation. The gas/particle forcing function terms tend to have a stabilizing influence akin to the inclusion of viscous damping terms. The real gas iterative decode procedure for extracting physical variables from the conservation array, E, is described in Ref. 25.

Boundary Point Procedures

The code presently contains provisions for the following types of bounding surfaces: 1) geometric; 2) shock; 3) contact; and 4) characteristic. The noniterative predictor-corrector characteristic procedures employed for determining gas-phase properties at boundary points are straightforward and described in Refs. 10, 18, and 25. The particle-cloud equations at boundary points are solved by finite-difference procedures eliminating the cumbersome interpolative procedures entailed in particle characteristic techniques. Since particle-cloud properties change continuously through gas-phase discontinuities, the standard interior point integration procedure can be implemented, modified at boundaries so that both the predictor and corrector steps are taken with the same one-sided difference. In the multiple domain approach, tests are performed at each boundary point to ascertain whether the boundary comprises an inflow or outflow type of boundary for each particle size group, j. With σ designating the slope of a gas-phase discontinuity boundary separating domains L and $L+1$, the sign of the parameter

$$Q_{p_j}\cdot\hat{n} = U_{p_j}\sin\sigma + V_{p_j}\cos\sigma \quad (19)$$

determines the boundary type for group j. Thus, if this parameter is positive, jth particle properties are evaluated as upper boundary points in domain L (implementing backward differences), while if negative, particle properties are evaluated as lower boundary points in domain $L+1$ (implementing forward differences).

At geometric boundaries, the impingement of particles on surfaces is calculated by treating the surface as an outflow boundary, i.e., particles impinging are simply removed from the flow. The particle impingement properties then comprise boundary conditions for a subsequent two-phase viscous flow problem. For problems initialized with particles adjacent to a geometric surface, if the surface variation is smooth and slowly varying in comparison to typical particle equilibration lengths, the boundary condition $\bar{Q}_{p_j}\cdot\hat{n}=0$ is imposed. This is accomplished[10,18] by first calculating particle properties using one-sided differences, and then rotating the predicted particle velocity vector to be parallel to the surface and correcting the particle-cloud density for the rotation. If the geometric surface is a centerbody of small radius r_L, the standard one-sided difference procedure does not reduce to the proper axisymmetric limit as $r_L\to 0$. The appropriate difference formulation is given in Refs. 10 and 18.

Limiting Particle Streamlines

In most gas/particle flows, the flow domain occupied by the various particle groups is less than the entire flow region being calculated. Previous supersonic flow models require the use of limiting streamlines where boundaries occupied by the various particle groups are formally traced throughout the flowfield. This cumbersome procedure is not required in SCIPPY. Here, particles are assumed to be present at all grid points in the flowfield. For those grid points containing no particles, the particle-cloud density is set equal to a small positive constant (effectively zero) and particle properties are equilibrated with those of the gas phase. The particle equations are integrated at all grid points; however, the more time-consuming task of evaluating the drag and heat-transfer coefficients is performed only if a preset minimal level of nonequilibrium exists (i.e., this task is avoided in nonparticulate regions and where smaller particle size groups have locally equilibrated).

In this approach, the interface between particulate and nonparticulate regions tends to become somewhat diffuse. A sharper interface is provided by a cutoff procedure whereby the particle-cloud density at initially nonparticulate grid points is maintained at the effective zero value until a prescribed minimal level is predicted (see Ref. 10). Similarly, for particulate grid points being depleted of particles, the cloud density is set to the effective zero value when it falls below this prescribed minimal level. Note that this approach provides for the separation of particles from solid surfaces with no additional logic required. Thus, in regions of rapid wall expansion, the grid points in the vicinity of the wall will become depleted of particles as part of the normal computational sequence. Small-angle reattachment is naturally accommodated by use of the $\bar{Q}_{p_j}\cdot\hat{n}=0$ boundary condition, while larger-angle impingement would necessitate removing the impinging particles from the flow as discussed above.

Specialized Procedures

External Flow Rules

For the analysis of plumes exhausting into supersonic streams, provisions are contained in SCIPPY to employ simple pressure/flow-deflection rules along the plume interface as a user option (in place of solving the bow shock layer via the multiple domain methodology described previously). Existing supersonic flow rules[26,27] are not descriptive of the plume nose region where a transition occurs from a locally two-dimensional solution at the nozzle lip to an axisymmetric solution downstream of the lip region. Assessment studies have indicated that a combination of the

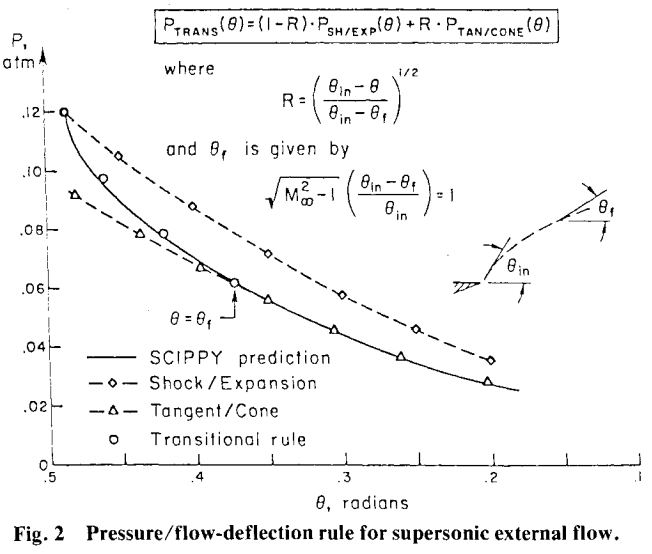

Fig. 2 Pressure/flow-deflection rule for supersonic external flow.

shock/expansion and tangent cone rules can be used to adequately predict the pressure distribution in the plume nearfield. Figure 2 displays the SCIPPY predicted pressure variation along a plumelike body in a Mach 4.5 external stream, which is compared with pressure distributions determined using simplified rules over the same plume geometry. It is seen that the shock/expansion rule overpredicts the pressure level in most of the nose region, since axisymmetric effects have not been accounted for while the tangent cone rule yields the best overall results except in the immediate lip region where the flow is locally two dimensional. These two rules are combined in a transitional region extending from the lip, θ_{in}, to an angle, θ_f, as given by the relation

$$P(\theta) = (1-R)P_{\text{shock/exp}} + R \cdot P_{\text{tan-cone}} \tag{20}$$

where $R = \sqrt{(\theta_{in}-\theta)/(\theta_{in}-\theta_f)}$, and θ_f is given by $\theta_f = \theta_{in}(1 - 1/\sqrt{M_\infty^2 - 1})$. For detached shocks, the 2-D solution at the lip is given by the tangent wedge rule. The tangent cone rule incorporated employs least-square polynomial fits of the exact nonlinear conical flow solutions.[25]

For hypersonic external streams, a unified Newtonian/Prandtl-Meyer relation[28] is employed, given by

$$P(\theta) = P_s \cdot \exp[\tilde{\theta}(0.456 - 1.47\tilde{\theta}) - 0.191] \tag{21}$$

where $P_s \sim \gamma_\infty P_\infty M_\infty^2$ and $\tilde{\theta} = \pi/2 - \theta$. A realistic representation of the hypersonic flowfield external to the plume requires provisions for including the effects of plume-induced separation which can be quite important at altitudes above 30 km.[29] Such capabilities are not yet incorporated in SCIPPY.

For plumes exhausting into a quiescent stream, the pressure is maintained constant along the plume interface, while for plumes exhausting into subsonic/transonic external streams, the pressure distribution is imposed as determined from the South-Jameson relaxation model.[30] The iterative approach described in Ref. 6 is employed for this latter analysis, which can account for the viscous displacement effect of jet entrainment.[5]

Embedded Subsonic Regions

In axisymmetric supersonic flows, the nonlinear strengthening of shock waves in propagating toward the axis precludes the occurrence of a regular reflection from the centerline and a triple-point configuration occurs (Fig. 3) yielding an embedded region of subsonic flow behind the Mach disk. The subsonic flow in the Mach disk streamtube is accelerated to supersonic velocity via the combined influence of inviscid (wave) and viscous (turbulent mixing) processes[31] as well as by gas/particle interactions for two-phase flows. The relative contribution of viscous and inviscid processes in accelerating the flow is dependent on the viscous/inviscid length scales with inviscid processes dominating for larger-sized Mach disks and turbulent mixing processes dominating as the Mach disk radius becomes negligibly small.

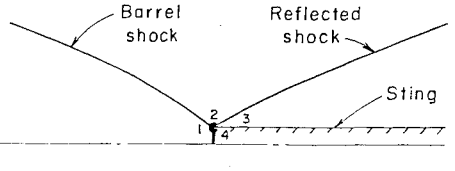

a) Sting approach for small Mach discs

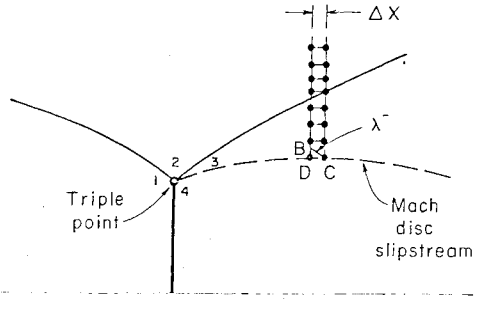

b) Abbett approach for large Mach discs

Fig. 3 Options for small and large Mach disks.

Restricting our attention to single-phase flows, Mach disk positions in SCIPPY are determined via the inviscid approach introduced by Abbett,[15] which has been demonstrated to yield positions comparing quite favorably with experimental data in a number of previous studies.[16,32,33] In the Abbett approach, the flow which has traversed the Mach disk is treated as a one-dimensional, isentropic streamtube with the correct Mach disk location being that which allows the subsonic flow in this streamtube to accelerate smoothly through a sonic throat. Turbulent mixing processes along the Mach disk slipstream and chemical relaxation processes in the Mach disk streamtube are accounted for in a subsequent analysis, which is discussed in Refs. 2 and 9.

For smaller-sized disks (i.e., those comparable in size to several radial grid intervals), the inclusion of viscous processes will tend to shift the inviscidly determined position downstream, and thus reduce the already small Mach disk radius. This effect is not presently accounted for and a sting default option is implemented when small disk sizes are predicted (as will be discussed below) which suffices for many engineering purposes. The inclusion of gas/particle interactions in the Mach disk streamtube, while potentially of great significance in the acceleration process, is not yet incorporated in SCIPPY. For two-phase flows, the analysis is presently limited to smaller-sized Mach disks where the sting option is implemented. The extension of SCIPPY to analyze nonequilibrium gas/particle interactions in the Mach disk streamtube in the inviscid limit is discussed in Refs. 18 and 25, while the viscous analysis, employing the fully coupled version of SCIPPY,[8,9] is discussed in Ref. 18.

In SCIPPY, embedded shocks propagating toward the axis, which will ultimately collapse into the triple-point configuration of Fig. 3, are numerically captured. The triple-point solution, however, is arrived at by formally solving the shock jump relations. The first step in the triple-point procedure involves identifying downrunning captured shocks (see Refs. 7 and 25) and obtaining properties both upstream [point 1] and downstream [point 2]. Then, properties behind the Mach disk [point 4] are determined from the normal shock jump relations from state 1 (if properties vary between the axis and point 1, averaging is required), while properties downstream of the reflected shock [point 3] are determined from the oblique shock relations, stipulating that $P_3 = P_4$. All shock jump solutions assume the composition to be chemically frozen across the shock.

Automated Mach Disk Analysis

The Mach disk solution in SCIPPY is fully automated (i.e., the code internally determines the Mach disk location through an iterative sequence of calculations requiring no user interface or input parameters). The automation involves: 1) selecting a first trial Mach disk location which must be upstream of the correct location and storing the flowfield data at that station; 2) advancing the solution downstream until a subsonic-to-subsonic streamtube transition occurs at a minimum area cross section; 3) repeating this process with trial locations selected at subsequent integration steps until a choking solution is detected; and 4) "forcing" the solution through a sonic throat via a fine-tuning procedure based on perturbing the initial Mach disk slipstream angle. The specific details of this automated procedure and the various controlling parameters involved (determined on the basis of trial calculations) are described in Refs. 7 and 25. These parameters have been improved by Wilmoth[34] to yield greater

efficiency (i.e., the new parameter controlling the first trial location places it closer to the correct solution, reducing the number of iterations entailed) and reliability for conditions pertinent to aircraft exhausts.

There are two other Mach disk options in SCIPPY—one is user initiated and the other is an internal default option. In the user-specified "sting" option, the Mach disk is dropped at the position where the triple-point solution (Fig. 3) yields an initial Mach disk slipstream angle of zero (i.e., $\theta_{1/4}=0$, $P_3=P_4$). A cylindrical sting whose radius equals that of the Mach disk is inserted into the flow at this station and the exhaust flow crossing the disk is ignored. This option is implemented when it is known, a priori, that disk sizes will be small (namely, for modestly underexpanded plumes with small nozzle lip angles) or when a "quick and dirty" calculation suffices (such as in plume studies keyed to signature prediction[3]). For flows with weak downrunning shocks, the nonlinear axisymmetric strengthening of the shock in approaching the axis may occur over a transverse length scale comparable to a grid interval. In the Abbett procedure, this is indicated by the nonoccurrence of a choking solution in all trial solutions attempted until the shock reaches the second grid point. In the sting option, the Mach disk slipstream angle, $\theta_{1/4}$, which decreases uniformly as the shock approaches the axis, is still positive at the second grid point. In both of these situations, a regular reflection default option is implemented whereby the downrunning shock is regularly reflected off of an inserted cylindrical sting whose radius is set equal to that of the second grid point. In this default option, properties behind the reflected shock are established by the requirement that $\theta_{1/4}=0$ and thus $P_3\neq P_4$.

Calculations

SCIPPY has been employed for numerous predictions of inviscid rocket and aircraft plume flowfields as well as for the prediction of various ducted flows (nozzles, diffusers, etc.). In this section, a handful of these calculations are presented which best exhibit specific capabilities of SCIPPY, demonstrate unique aspects of plume flowfields, and, hopefully, reinforce some of the technical details presented above. For a more complete description of inviscid SCIPPY calculations, the reader is referred to the references cited below.

Mach 2 Jet into Still Air—Multiple Cell Structure

Imperfectly expanded jets exhausting into still air are characterized by a multiple-cell structure associated with a repetitive sequence of expansion and compression waves. This characteristic pattern is exhibited by the calculation of an underexpanded Mach 2 jet (uniform exhaust, static pressure ratio of 2, $\gamma=1.4$), whose predicted centerline pressure variation is given in Fig. 4 for five inviscid cells (the labeled pressure peaks signify the end of inviscid cells, while the minimum points are the Mach disk locations).

The calculation used 41 grid points in a single mapped domain bounded by the axis and plume interface and implemented the sting Mach disk option. The significant damping of the peak pressure levels in the first three inviscid cells is attributable to finite strength shock waves (i.e., to shock-induced viscous dissipation). Beyond the third cell, wave processes are essentially linear and the slow decay in peak (maxima and minima) pressure levels (as indicated by the dashed lines) is attributable to the numerical viscosity implicit in the MacCormack algorithm. In all calculations presented, the standard algorithm has been employed and no additional artificial viscosity terms were introduced.

With the ability to perform multiple-cell calculations exhibited (in the limit of small Mach disk sizes), the accuracy of this type of calculation is exhibited by a second calculation, performed with the static pressure ratio reduced to 1.445 to conform to the experimental measurements of Ref. 36. In this case, the sting criterion could not be satisfied (using the maximum number of radial grid intervals (80) presently available) and the regular reflection default option was implemented. The predicted axial pressure variation is compared with experimental data[36] in Fig. 5. The agreement is quite good for the first two inviscid cells. The physical damping of pressure excursions due to viscous (mixing) effects is clearly exhibited in the experimental data. Beyond the second inviscid cell, the SCIPPY predictions overestimate the pressure levels and predict peak locations downstream of the measured peaks. Such behavior is expected since the numerical damping implicit in SCIPPY is negligible with respect to physical levels and the curvature of the shock waves in traversing through the plume shear layer to the viscous sonic line is not accounted for. This issue has been addressed in the survey paper of Ref. 27, where the inability of inviscid plume solutions to duplicate multiple-cell laboratory data for rocket plumes beyond the second cell is examined and in Ref. 36 for studies keyed to shock noise in jets. The viscous extension of the SCIPPY model[8,9] presently under development, will have the ability to account for these processes.

Mach 3 Jet—Comparison with Shock-Fitting Solutions

Comparisons have been made with solutions reported in Ref. 16 employing a shock-fitting procedure, to exhibit that shock-capturing and shock-fitting techniques can yield results of comparable quality. The first case is that of an underexpanded Mach 3 jet (uniform exhaust, static pressure ratio of 4, $\gamma=1.4$) exhausting into still air. Predicted flowfield schematics for both solutions are given in Fig. 6 indicating principal discontinuity surfaces. The SCIPPY prediction was performed with 41 grid points and one domain. Both predictions employed the Abbett procedure for locating the Mach disk. The two predictions are seen to yield comparable results including analogous Mach disk and sonic throat locations.

In the second case, the same Mach 3 jet exhausts into a Mach 2 airstream with an exit static pressure ratio of 15. The SCIPPY prediction employed two domains (domain 1 extended from the axis to the plume interface and domain 2 extended from the interface to the fitted bow (external) shock)

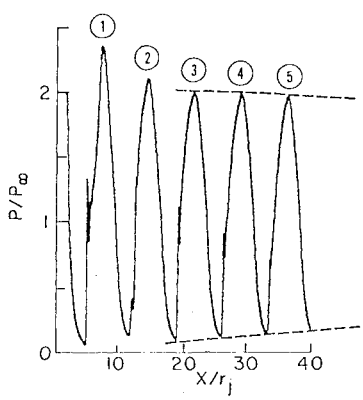

Fig. 4 Predicted axial pressure variation for Mach 2 jet into still air ($P_j/P_\infty=2$) for five inviscid cells.

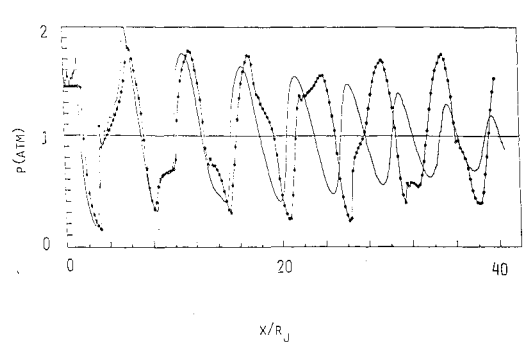

Fig. 5 Comparison of predicted and measured axial pressure variations for Mach 2 jet into still air ($P_j/P_\infty=1.45$, from Ref. 36).

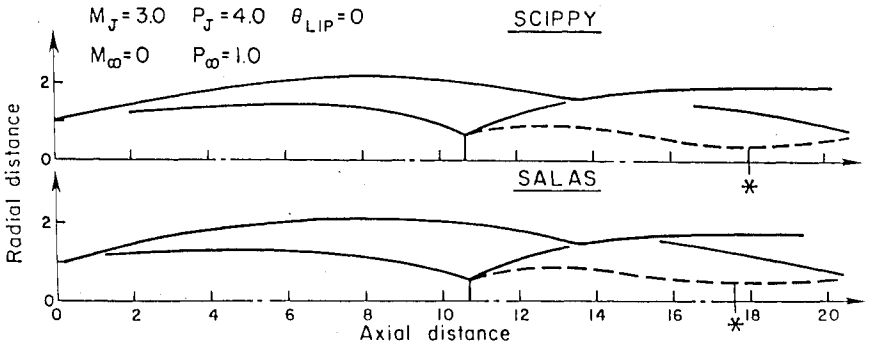

Fig. 6 Comparison of SCIPPY shock-capturing and Salas shock-fitting predictions for Mach 3 jet into still air.

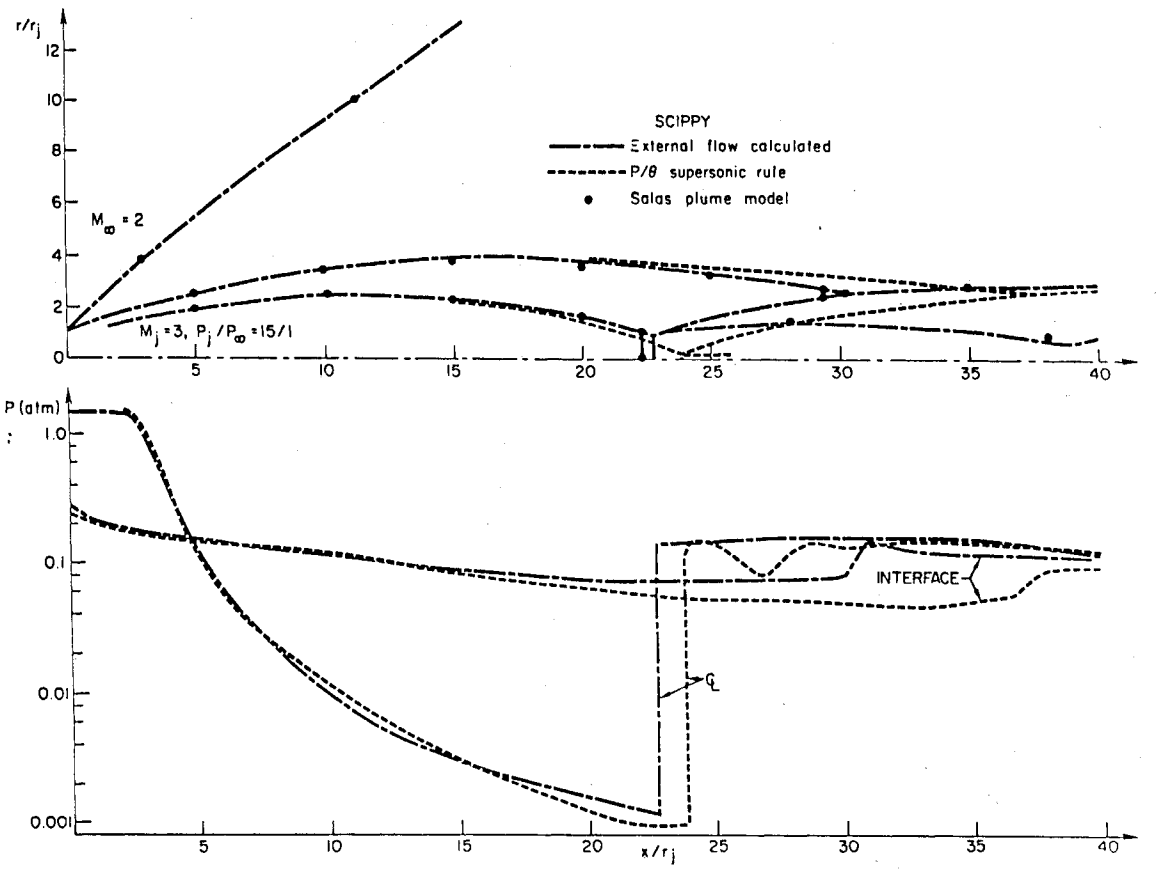

Fig. 7 Mach 3 jet into Mach 2 external stream. Comparison of SCIPPY one- and two-domain predictions and Salas prediction.

and is seen to be in good agreement with the Salas plume model prediction,[16] as depicted in Fig. 7. Also depicted is a SCIPPY prediction employing a one-domain approach (axis to interface) using the supersonic pressure/flow deflection rule described above along the interface. While the predicted pressure levels along the plume interface appear quite reasonable employing this P/θ rule, the results in the vicinity of the Mach disk are quite different (the one-domain calculation predicts a Mach disk location well downstream of the two-domain calculation and a substantially smaller Mach disk size). Since the exhaust flow representation is identical in both the one- and two-domain calculations, one must infer that the Mach disk solution is extremely sensitive to the representation of the external flow. This implies that a realistic treatment of the flowfield around the missile, including a detailed treatment of the base and/or plume-induced separated region, can be an important factor in obtaining an accurate portrayal of the flowfield within the plume.

Two-Dimensional Duct—Comparison with Shock-Fitting Solution

This case involves the prediction of a two-dimensional ducted flow with multiple shock reflections. The initial conditions were uniform ($M = 2.94$, $P = 845.5$, $\gamma = 1.4$) and the wall geometry is given in Ref. 25. The shock propagation pattern and predicted pressure distributions along the upper and lower walls are depicted in Fig. 8. SCIPPY shock-capturing predictions with 11 and 21 radial grid points are seen to compare favorably with the shock-fitting predictions of the SEAGULL code.[37] All grid points are indicated for the SCIPPY 11-point calculation, and all grid points in the vicinity of shock reflection points for the 21-point calculation. Of particular significance in the SCIPPY predictions is the absence of pressure overshoots at shock reflection points and the negligible numerical damping.

Amine Booster at Low Altitudes

A series of inviscid plume predictions were performed for an amine booster at altitudes of 5, 15, 25, 35, 50, and 70 km, and typical flight conditions, exhibiting the ability of SCIPPY to encompass the full range of conditions encounterable at low altitudes (0-70 km). In these calculations, sensitivities were exhibited to real vs perfect gas solutions, Abbett vs sting Mach disk solutions, uniform vs nonuniform exhaust representations, and to the external flow solution. In addition, comparisons were made with the MAXIPLUM code[38]

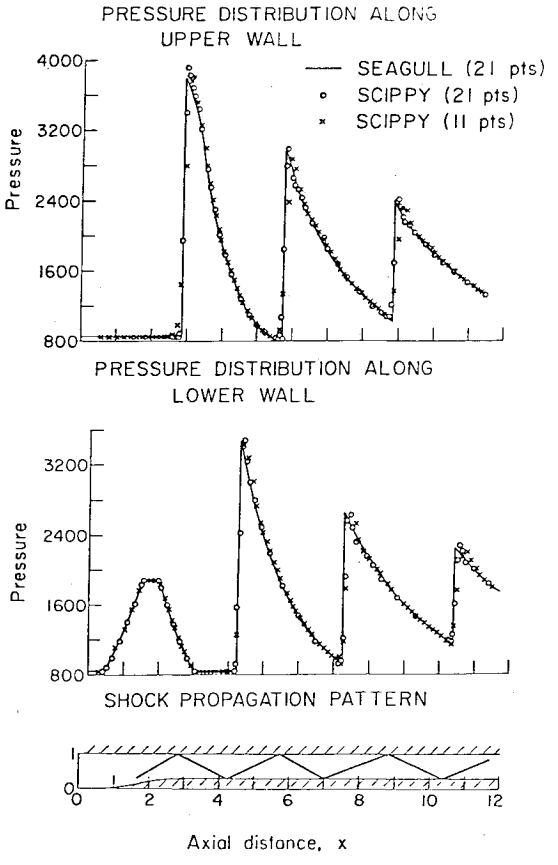

Fig. 8 Two-dimensional supersonic duct flow, SCIPPY shock-capturing and SEAGULL shock-fitting predictions.

which implements a multiple-domain shock-fitting methodology in spherical coordinates. The details of all these calculations are given in Refs. 24 and 25 and are too lengthy to include in this article.

The 70-km calculation has been selected for presentation here. Figure 9 depicts predicted flowfield schematics for real and perfect gas solutions using both the Abbett and sting Mach disk options. All predictions implemented the Newtonian/Prandtl-Meyer relation of Eq. (21) in representing the external flow. Uniform (conical) exhaust conditions ($M=3.1$, $T=1850$ K, lip angle = 10 deg) were employed with a Mach 8 external stream and exit static pressure ratio of 1700. The exhaust composition (mole fractions) is given by CO = 0.0485, $CO_2=0.0835$, H = 0.00025, $H_2=0.0614$, $H_2O=0.45$, $N_2=0.3562$, and OH = 0.00015; a γ of 1.23 was implemented in the perfect gas solutions.

The plume is seen to be quite large at 70 km with an inviscid first cell length of approximately 500 exit radii and a maximum transverse width of 60 radii. The sting Mach disk locations are well downstream of locations predicted using the Abbett procedure yielding substantially smaller Mach disk radii. All shock-induced entropy production generally occurs in the first inviscid cell for cases such as this (see Ref. 27) and practical inviscid calculations can be terminated at the Mach disk sonic throat. In this nearfield region, viscous (turbulent mixing) processes are confined to thin mixing layers growing along the plume and Mach disk slipstreams and are presently analyzed by the overlaid (uncoupled) procedure described in Refs. 2 and 9. The smoothly varying pressures along both of these slipstreams permits use of this type of viscous/inviscid uncoupling. However, the significant negative displacement effect due to wakelike mixing and chemical relaxation behind the Mach disk may indicate a requirement for a higher level of coupling in this region.

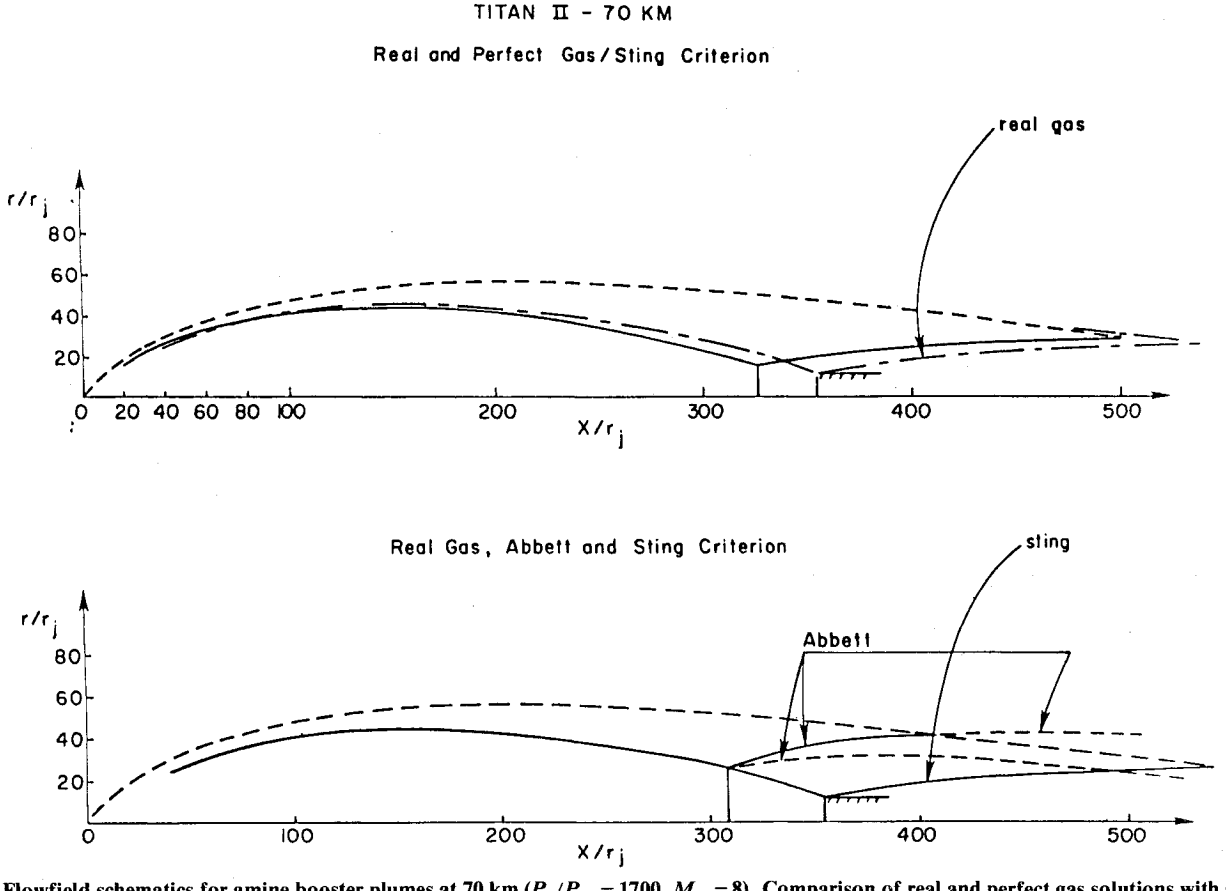

Fig. 9 Flowfield schematics for amine booster plumes at 70 km ($P_j/P_\infty=1700$, $M_\infty=8$). Comparison of real and perfect gas solutions with sting option and Abbett and sting solutions with real gas option.

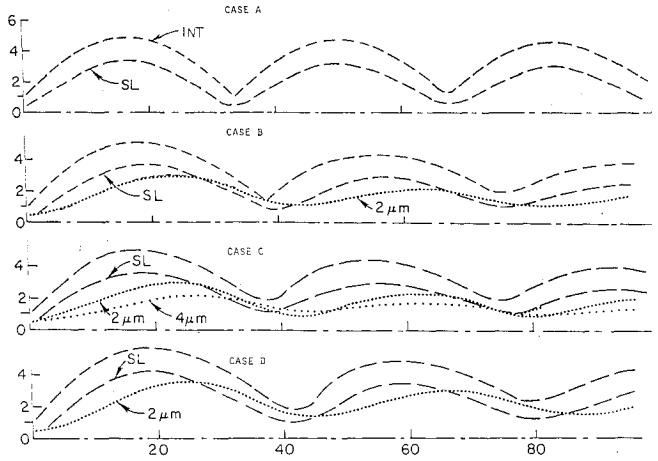

Fig. 10 Multiple-cell flowfield schematics for Mach 2.4 two-phase planar jet exhausting into still air ($P_j/P_\infty = 4$, $r_j = 0.3$ m). Case A—single-phase calculation; case B—15 % loading of 2 μm particles initially equilibrated with gas; case C—7.5% loading of 2 and 4 μm particles initially equilibrated with gas; case D—15% loading 2 μm particles initially out of equilibrium.

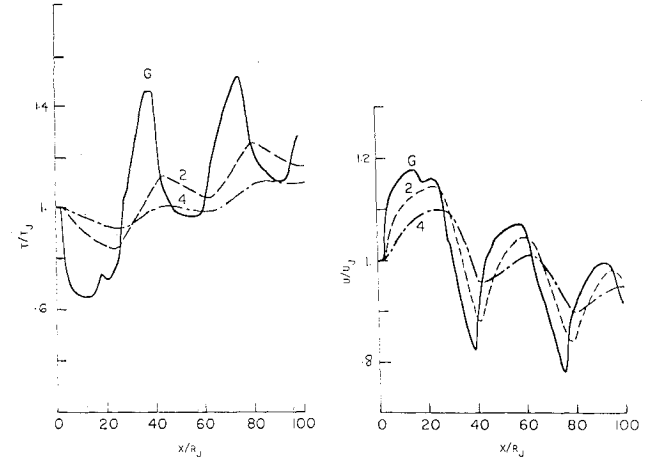

Fig. 11 Predicted symmetry plane velocity and temperature variations for gas (*G*) and particle (2,4) phases for case C.

Two-Phase Jets

A series of multiple-cell calculations (detailed in Ref. 25) for two-phase Mach 2.4 underexpanded planar jets ($T_j = 1000$ K, $P_j = 1$ atm, $\gamma = 1.4$) exhausting into still air ($P_\infty = 0.25$ atm) serve to demonstrate the basic features of gas/particle nonequilibrium in inviscid exhaust flows. A planar configuration was selected to avoid the additional complexities introduced by the presence of Mach disks. Flowfield schematics for cases A-D are given in Fig. 10. Case A is a single-phase calculation; in case B, a 15% mass loading (typical loadings in rocket exhausts vary from 0 to 30%) of 2 μm radius (typical particle sizes of interest range from 0.5 to 10 μm) Al_2O_3 particles is uniformly distributed across half the nozzle exit plane (i.e, from $r = 0$ to 0.15 m) and initially equilibrated with the gas; in case C, the same overall loading and spatial distribution as case B is employed with a size distribution of 2 and 4 μm particles (7.5% of each); in case D, the same distributions as B are employed with the 2 μm particles initially out of equilibrium with the gas ($T_p = 1.2\ T_{gas}$, $U_p = 0.8\ U_{gas}$). All predictions implemented the Henderson[22] drag correlations.

Referring to Fig. 10, the single-phase jet prediction (case A) depicts the variation of the plume interface (INT) and the streamline emanating from the half-radius position at the nozzle exit plane (SL). A repetitive pattern for three inviscid cells is exhibited. With the introduction of particles (case B),

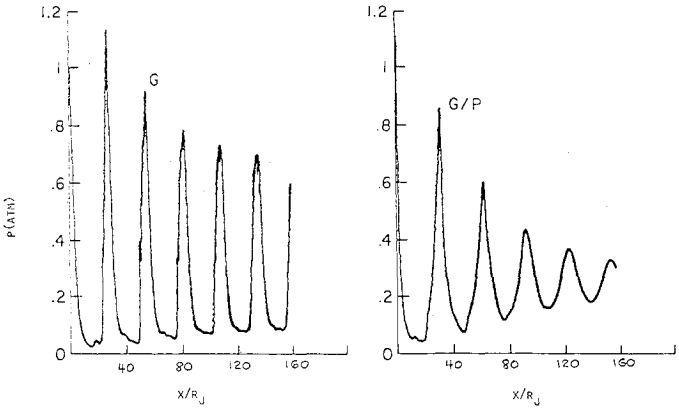

Fig. 12 Comparison of symmetry plane pressure variations for case A (*G*) and case D (*G/P*) predictions.

the inviscid plume pattern shifts with cell lengths elongated by about 15%. The limiting particle streamline (2 μm) cannot abruptly turn through the initial Prandtl-Meyer fan and thus lags behind the gas-phase streamline (which emanated from the same position) quite noticeably. This occurs for all successive waves in the flowfield with the path to equilibrium continuously disrupted by the passage of new waves.

In case C, the geometric lag of the 4 μm particles is seen to be substantially greater than that of the 2 μm particles (Fig. 10). The difference in lag effects between the 2 and 4 μm particle groups is exhibited by the symmetry plane variations of velocity and temperature shown in Fig. 11 with one net result being the continual generation of entropy through the mechanism of drag-induced viscous dissipation. The most pronounced effect of gas-particle interactions is exhibited in case D, where the gas and particle phases are initially out of equilibrium at the nozzle exit plane. The symmetry plane pressure variations for this case (carried out to 200 exit radii) are compared with those for single-phase flow (case A) in Fig. 12. After the third inviscid cell (i.e., third peak), the damping in peak pressure levels for the single-phase calculation becomes negligible. The damping due to gas/particle interactions in the two-phase calculation is continual with pressure excursions (ratio of maximum to minimum levels) of less than 1.5 encountered at 200 (in comparison with excursions in excess of 10 for the single-phase calculation at this location).

Concluding Remarks

The SCIPPY shock-capturing model for steady, supersonic, one- and two-phase flows has been described. Unique features such as the mapped multiple-domain approach and automated Mach disk procedure provide for the accurate analysis of complex exhaust flowfields. The fully coupled nonequilibrium treatment of gas/particle interactions is quite effective in analyzing flows with multiple discontinuities. Calculations described compare favorably with shock-fitting predictions and available nearfield data. Further calculations for one- and two-phase plumes, nozzles, and diffusers are described in the referenced literature. Extensions of the inviscid SCIPPY model to problems such as high-altitude plumes[25] (using mapped spherical coordinates) and highly curved wall jets[39] (using mapped surface normal coordinates) have recently been formulated.

The calculation of realistic exhaust flowfields requires the consideration of both viscous (turbulent mixing) and chemical processes. SCIPPY is presently incorporated in computational systems where it interfaces with viscous solutions via an overlaid procedure for situations where viscous/inviscid coupling is weakly interactive (see Refs. 1-3, 9, and 24 for rocket exhausts and Refs. 5-7 for aircraft exhausts). A fully coupled viscous extension of SCIPPY has been formulated and applied to several strongly interactive supersonic

mixing problems as described in Refs. 8 and 9. Work is progressing in this area under a program supported by NASA/LRC. Realistic two-phase exhaust solutions require addressing the complex problems of turbulence/particle interactions and the treatment of gas/particle nonequilibrium behind Mach disks as discussed in Refs. 18 and 40. Work is also progressing in this area under MICOM support.

Acknowledgments

This work was supported by the JANNAF Exhaust Plume Technology Subcommittee under MICOM Contract No. DAAK40-78-C-0124 monitored by Dr. B. J. Walker. The authors express their thanks to Mr. R. J. Prozan of Continuum, Inc., Huntsville, Ala., Dr. R. G. Wilmoth of NASA/LRC, and Mr. H. S. Pergament of Science Applications, Inc., Princeton, N.J., for many helpful discussions.

References

[1] Dash, S. M., Pergament, H. S., and Thorpe, R D., "The JANNAF Standard Plume Flowfield Model: Modular Approach, Computational Features and Preliminary Results," *JANNAF 11th Plume Technology Meeting*, May 1979, CPIA Pub. 306, Vol. I, pp. 345-442.

[2] Dash, S. M. and Pergament, H. S., "The JANNAF Standard Plume Flowfield Model: Operational Features and Preliminary Assessment," *JANNAF 12th Plume Technology Meeting*, CPIA Pub. 332, Vol. II, Colo., Nov. 1980, pp. 225-288.

[3] Dash, S. M., Pearce, B. E., Pergament, H. S., and Fishburne, E. S., "Prediction of Rocket Plume Flowfields for IR Signature Studies," *Journal of Spacecraft and Rockets*, Vol. 17, May 1980, pp. 190-199.

[4] Dash, S. M., Pergament, H. S., and Thorpe, R. D., "A Modular Approach for the Coupling of Viscous and Inviscid Processes in Exhaust Plume Flows," AIAA Paper 79-0150, Jan. 1979.

[5] Dash, S. M., Wilmoth, R. G., and Pergament, H. S., "An Overlaid Viscous/Inviscid Model for the Prediction of Nearfield Jet Entrainment," *AIAA Journal*, Vol. 17, Sept. 1979, pp. 950-958.

[6] Wilmoth, R. G. and Dash, S. M., "A Viscous-Inviscid Interaction Model of Jet Entrainment," *AGARD Symposium on Computation of Viscous-Inviscid Interactions*, Colorado Springs, Colo., AGARD-CP-291, Sept. 1980, pp. 13.1-15.

[7] Dash, S. M., Pergament, H. S., and Thorpe, R. D., "Computational Models for the Viscous/Inviscid Analysis of Jet Aircraft Exhaust Plumes," NASA CR 3289, May 1980.

[8] Dash, S. M., "Preliminary Calculations of Supersonic Viscous/Inviscid Interactions Using the Fully-Coupled Version of the SCIPPY Code," Aeronautical Research Associates of Princeton, TM No. 79-3, Feb. 1979.

[9] Dash, S. M. and Pergament, H. S., "A Computational System for the Analysis of Mixing/Chemical/Shock Processes in Supersonic Internal and Exhaust Plume Flowfields," AIAA Paper 80-1255, June 1980.

[10] Dash, S. M., "A Two-Phase Flow Version of SCIPPY for the Analysis of Supersonic Exhaust Plumes, Nozzles and Diffusers," Aeronautical Research Associates of Princeton, Rept. No. 426, Sept. 1980.

[11] MacCormack, R. W., "The Effect of Viscosity in Hypervelocity Impact Cratering," AIAA Paper 69-354, May 1969.

[12] Dash, S. M. and Del Guidice, P. D., "Numerical Methods for the Calculation of Three-Dimensional Nozzle Exhaust Flowfields," *Aerodynamic Analyses Requiring Advanced Computers*, NASA SP-347, Vol. I, March 1975, pp. 659-701.

[13] Dash, S. M. and Del Guidice, P. D., "Analysis of Three-Dimensional Ducted and Exhaust Plume Flowfields," *AIAA Journal*, Vol. 16, Aug. 1978, pp. 823-830.

[14] Abbett, M. J., "Boundary Condition Calculational Procedures for Inviscid Supersonic Flowfields," *AIAA Computational Fluid Dynamics Conference Proceedings*, July 1973, pp. 153-172.

[15] Abbett, M. J., "Mach Disc in Underexpanded Exhaust Plumes," *AIAA Journal*, Vol. 9, March 1971, pp. 512-514.

[16] Salas, M. D., "The Numerical Calculation of Inviscid Plume Flowfields," AIAA Paper 74-523, June 1974.

[17] Thorpe, R. D., Dash, S. M., and Pergament, H. S., "Inclusion of Gas/Particle Interactions in a Shock Capturing Model for Nozzle and Exhaust Plume Flows," AIAA Paper 79-1288, June 1979.

[18] Dash, S. M., "Computational Methodology for the Inclusion of Gas/Particle Nonequilibrium Effects in Exhaust Flowfields," *JANNAF 12th Plume Technology Meeting*, Nov. 1980, CPIA Pub. 332, Vol. II, pp. 289-350.

[19] Schaff, S. and Chambre, R., "Flow of Rarefied Gases," in *Fundamentals of Gas Dynamics*, Princeton Series, Vol. III, Princeton University Press, Princeton, N.J., 1958.

[20] Salita, M., "Examination of Recent Models for Particle Drag in Nozzle Flows," Thiokol/Wasatch Division, Brigham City, Utah, Interoffice Memo No. 2814-79-M105, Aug. 1979.

[21] Nickerson, G. R., Coats, D. E., and Hermsen, R. W., "Solid Propellant Rocket Motor Performance Predictions Using the Improved SPP Computer Model," *16th JANNAF Combustion Meeting*, Sept. 1979, CPIA Pub. 308, Vol. III, pp. 413-428.

[22] Henderson, C. B., "Drag Coefficients of Spheres in Continuum and Rarefied Flows," *AIAA Journal*, Vol. 14, June 1976, pp. 707-708.

[23] Gordon, S. and McBride, B. J., "Computer Program for Calculation of Complex Chemical Equilibrium Compositions, Rocket Performance, Incident and Reflected Shocks and Chapman-Jouguet Detonations," NASA SP-237, 1971.

[24] Dash, S. M., Pergament, H. S., Thorpe, R. D., Abuchowski, S. A., and Hussain, J. C., "Operational Instructions for a Preliminary Version of the JANNAF Standard Plume Flowfield Model (SPF/1)," Aeronautical Research Associates of Princeton, Rept. No. 415, March 1980.

[25] Dash, S. M. and Thorpe, R. D., "A Shock Capturing Model (SCIPPY) for the Analysis of Steady Supersonic One and Two Phase Flows," AIAA Paper 80-1254, July 1980.

[26] Hayes, W. D. and Probstein, R. F., *Hypersonic Flow Theory*, Vol. I, Inviscid Flows, 2nd ed., Academic Press, New York, N.Y. 1966.

[27] Dash, S. M. and Pergament, H. S., "The Analysis of Low Altitude Rocket and Aircraft Plume Flowfields: Modeling Requirements and Procedures," *JANNAF 10th Plume Technology Meeting*, Sept. 1977, CPIA Pub. 291, Vol. I, pp. 53-132.

[28] Vaglio-Laurin, R. and Trella, M., "A Study of Flowfields About Some Typical Blunt-Nosed Slender Bodies," *Aerospace Engineering*, Vol. 20, 1961, pp. 20-21 and 80-88.

[29] Schulz, R. J. and Bauer, R. C., "Rocket Plume Testing in Ground Test Facilities," *Journal of Spacecraft and Rockets*, Vol. 11, Jan. 1974, pp. 16-20.

[30] South, J. D. and Jameson, A., "Relaxation Solution for Inviscid Axisymmetric Transonic Flow Over Blunt or Pointed Bodies," *Proceedings of AIAA Computational Fluid Dynamics Conference*, July 1973, pp. 8-17.

[31] Back, L. H. and Cuffel, R. B., "Viscous Slipstream Flow Downstream of a Centerline Mach Reflection," *AIAA Journal*, Vol. 9, Oct. 1971, pp. 2107-2109.

[32] Chang, I. S. and Chow, W. L., "Mach Disc from Underexpanded Axisymmetric Nozzle Flow," *AIAA Journal*, Vol. 12, Aug. 1974, pp. 1079-1082.

[33] Fox, J. H., "On the Structure of Jet Plumes," *AIAA Journal*, Vol. 12, Jan. 1974, pp. 105-107.

[34] Wilmoth, R. G., personal communication, NASA Langley Research Center, Hampton, Va., Dec. 1980.

[35] Dash, S. M. and Thorpe, R. D., "A New Shock-Capturing/Shock Fitting Computational Model for Analyzing Supersonic Inviscid Flows (The SCIPPY Code)," Aeronautical Research Associates of Princeton, Rept. No. 366, Nov. 1978.

[36] Seiner, J. M. and Norum, T. D., "Aerodynamic Aspects of Shock Containing Jet Plumes," AIAA Paper 80-0965, June 1980.

[37] Salas, M. D., "Shock Fitting Method for Complicated Two-Dimensional Supersonic Flows," *AIAA Journal*, Vol. 14, May 1976, pp. 583-588.

[38] Dash, S. M., Boccio, J., and Weilerstein, G., "A Computational System for the Prediction of Low Altitude Rocket Plume Flowfields: Volume II—Inviscid Plume Model (MAXIPLUM)," General Applied Science Laboratories, Inc., Westbury, N.Y., TR-239, Dec. 1976.

[39] Dash, S. M., "An Overlaid Procedure for the Viscous/Inviscid Analysis of Wall Jets," Science Applications, Inc., Princeton, N.J., TM-2, Dec. 1980.

[40] Dash, S. M., "Gas/Particle Interactions in Rocket Exhaust Plumes," *ARO Workshop on Multiphase Flow*, Ballistic Research Lab., Aberdeen Proving Ground, Md., Feb. 1981.